

Simulation Study of Energy Resolution with Changing Pixel Size for Radon Monitor Based on *Topmetal-II*⁻ TPC

Mengyao Huang^{1;1)} Hua Pei² Xiangming Sun^{2;2)} Shuguang Zou²

¹ Department of Physics and Astronomy, Iowa State University, Ames, Iowa 50010, USA

² College of Physical Science and Technology, Central China Normal University, Wuhan, Hubei 430079, China

Abstract: In this paper, we study how pixel size influences energy resolution for a pixelated detector – a proposed high sensitivity, low cost, and real time radon monitor based on *Topmetal-II*⁻ TPC. Although smaller pixel can generally achieve higher spatial resolution, electronic noise might come into play in worsening the energy resolution. Using Geant4-based simulation, we figure out to what extent it worsens the energy resolution. A non-monotonic trend is observed for energy resolution varies with pixel size for small pixel size region. After introducing an empirical expression, it can be shown that this variation is due to a combination effect of pixel size and threshold on pixel. The contribution of electronic noise to energy resolution for 400 μm pixel size and 1 σ threshold is 45 keV FWHM, which is comparable to the energy resolution causing by energy fluctuation in ionization process inside TPC ($\sim 20\text{keV}$). The analysis is useful in choosing suitable pixel size for future pixelated detectors.

Key words: Geant4 simulation, energy resolution, pixel size, radon monitor, Topmetal

PACS: 29.25.Rm, 29.40.Cs, 29.40.Gx, 29.40.Wk

1 Introduction

Radon-222 is a well-known carcinogen in the air. When radon gas is inhaled, alpha particles emitted by radon-222 and its progenies will interact with biological tissue in the lungs leading to DNA damage. It is reported by World Health Organization (WHO) that long-term lung cancer risk rises about 20% per 100 Bq/m³ increase in indoor radon exposure [1]. WHO propose a reference level of 100 Bq/m³ to minimize health hazards due to indoor radon exposure, while 200 Bq/m³ is advocated in many countries as an Action Level [1]. Indoor radon gas can be naturally released from soil adjacent to the foundation, construction materials, and tap water when it is supplied from groundwater in radium-bearing aquifers [2]. With 3.8-day half-life, radon-222 can easily transmit and concentrate in enclosed space. As a result, indoor radon level is generally much higher than outdoor. To ensure a safety living environment, it is essential to monitor radon concentration during and after constructing. Therefore, there is a need for an inexpensive, portable and real-time radon monitor for household and construction supervisor.

Pixelated TPC detectors have showed excellent performance in achieving high sensitivities in radon detection. Besides, the standard pixel foundry process also promising for reducing the cost. Radon level is determined by detecting alpha particles emitting by radon. These detectors make use of both spatial resolution and

energy resolution in determining signals, suppressing backgrounds to a level that do not require statistics subtraction. Companies using this technique includes XIA, which achieves a sensitivity of several alphas/m²/day for solid materials using pixel sensors with 12 mm on edge [3].

Recently, a pixel sensor *Topmetal-II*⁻ has been developed in Pixel Lab at Central China Normal University [4]. This sensor is assembled by the standard 0.35 μm CMOS Integrated Circuit process and can achieve a higher spatial resolution, with electronic noise lower than 15 e⁻. These properties make the sensor promising in detecting radon with higher sensitivities. However, electronic noise might come in to play an important role in worsening the energy resolution.

Thus, we want to explore to what extent the changing pixel size and threshold influence energy resolution caused by electronic noise for this radon detector, using a Geant4-based [5] simulation method. An non-monotonic trend of energy resolution for small pixel size region is analyzed.

1) E-mail: mengyaoh@iastate.edu

2) E-mail: xmsun@phy.cnu.edu.cn

2 Alpha-detecting *Topmetal-II*⁻ TPC

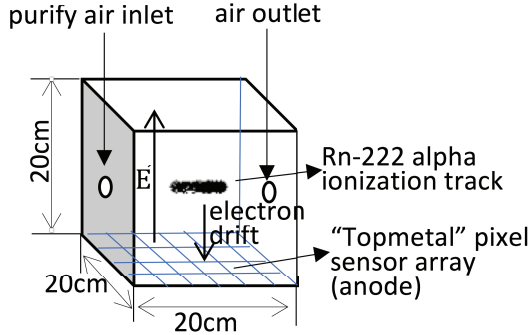


Fig. 1. A schematic view of radon alpha-detecting *Topmetal-II*⁻ TPC.

Fig. 1 is a schematic view of radon alpha-detecting *Topmetal-II*⁻ TPC. The $20 \times 20 \times 20$ cm³ cubic volume contains air sample, with *Topmetal-II*⁻ pixel sensor arrays placed on the bottom plane. A unique character of *Topmetal-II*⁻ sensor is that its top material is metal, which can be served as an electrode to generate electric field. An air supplier will be placed on the inlet for providing dry clean air into the volume. Inside the volume, a certain ratio of radon-222 nucleus decay to polonium-218, emitting alpha particles with energy of 5489 keV. The emitting alpha particles then interact with air molecules, producing ionization tracks. The ionized electrons (or corresponding ions) drift to the bottom plane due to the electric field and are collected by *Topmetal-II*⁻ pixel sensor array, on which the charge signals transfer into detectable pulse signals. To simplify our calculation, we will use the idealized “electron drift” model, instead of the more accurate “ion drift” model.

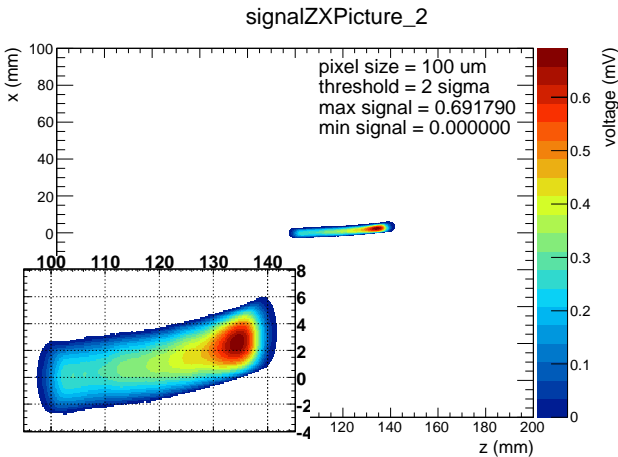


Fig. 2. Simulation signal on *Topmetal-II*⁻ pixel sensor array. The bottom left panel is an enlarged graph of the signal.

Fig. 2 is an example of simulation signal on *Topmetal-II*⁻ pixel sensor array, with length of side of each pixel $100 \mu\text{m}$ at threshold 2σ , where σ is defined as noise on pixel, which is about $15 e^-$ taken from the test result in [4]. In this paper, pixel size is characterized by length of side of pixel. The right color bar shows the signal intention scale in mV. Although the signal we use in our simulation is in unit of energy (keV), the charge conversion gain measured in [4] makes it possible to convert the energy to voltage. The average minimum ionization energy in the air is 0.0337 keV, i.e., 1 keV energy deposition in the air ionizes about $30 e^-$. For *Topmetal-II*⁻ charge conversion gain $32.8 e^-/\text{mV}$ [4], the conversion between keV and mV is almost 1:1. In Fig. 2, an alpha particle with energy of 5489 keV is shooting parallel to the bottom plane, along the z axis. The length of the ionization track is approximately 45 mm. Cutting out spaces that are 45 mm close to the boundary, it follows that the volume which enables an event to leave its whole track in the detector is about 1 liter. This means that the counting rate of radon-222 decay events is ~ 6 counts/min, at 100 Bq/m³ radon level. If functioning well, it might achieve a sensitivity of 3.6 CPH/Bq·m³.

3 The Simulation

Firstly, we use a Geant4-based package to generate alpha particles of 5489 keV inside the volume. Geant4 is a Monte Carlo framework for simulation of particle passage through matter. To speed up our analysis, we choose a cut-off energy greater than the minimum energy of producing an electron-ion pair in the air (W value), and we check that this change will not affect much of the shape and length of radon-emitting alpha ionization track. This is because the density of ionized electrons is high enough, which allows for clustering ionized electrons and using these series of clusters to represent the shape of the track. After creating the track, each ionization cluster is then divided by W value to get back the real number of ionized electrons. For simplicity, the ionized electrons are spread uniformly inside the cluster.

We assume that the diffusion of ionized electrons inside the TPC follows 3D diffusion equation, so the expected radius of an electron cluster after diffusion is

$$r = r_0 + \sqrt{6Dt}, \quad (1)$$

where r_0 is the initial radius of the cluster, D is the electron diffusion coefficient and t is the electron drift time. The electron drift time can be calculated from total drift length divided by drift velocity.

The electron diffusion coefficient D and the electron drift velocity can be simulated by Magboltz package [6]. The parameters of the air are input as a gas mixture containing 78.08% of N_2 , 20.95% of O_2 , 0.93% of Ar and

0.04% of CO₂. Under 100 V/cm vertical electric field, at room temperature (20 °C) and at standard pressure (760.0 Torr), the electron diffusion coefficient D is found to be 47890.0 mm²/s and the electron drift velocity is found to be 4573000.0 mm/s.

To create signals as what we would expect from the pixel sensors, we use code to make a 2D grid on the bottom plane, with the size of each griding cell equals to the size of pixel. For simplicity, we assume that there are no gaps between sensors, which means the whole 20×20 cm² bottom plane is sensitive to charges. Each electron is collected by the corresponding pixel right under its spatial position after diffusion. Then, Gaussian noise with mean value 0 and standard deviation 15 e⁻ is added on each cell to simulate the electronic noise of *Topmetal-II*⁻ pixel sensor. Here we assume that the energy of each electron when it reaches the bottom plane is the same as when it is created, as we neglect the recombination and decomposition during the drifting process. The effect of recombination and decomposition should not be ignored for a real detector, but in this paper, we only focus on dependence of energy resolution on parameters of the pixel, such as pixel size and threshold on pixel, thus the details in drifting process are not so important in our current discussion.

The output signal of each pixel is the original charge signal (O_Signal_n) subtracted by the threshold (T) placed on pixel.

$$O_Signal_n = Noise_n + Hit_Energy_n, \quad (2)$$

$$Signal_n = \begin{cases} O_Signal_n - T, & O_Signal_n > T \\ 0, & Otherwise \end{cases}. \quad (3)$$

where n runs along the corresponding ionization track. We assume that a track finding algorithm can be performed to separate tracks with 100% efficiency. There are two main reasons that lead us to do this assumption. First, as we force the threshold on each pixel to be greater than 1σ and less than the possible maximum signal on pixel, in statistics, this causes ~84.2% of noises be ruled out in areas that do not receive any ex-

ternal charge. Second, the advantage of time resolution of TPC provides 3-D imagine of an event thus further suppresses the noise.

To calculate the energy resolution, 1000 radon-alpha events are generated from the center of the detector volume with each alpha particle's energy equals to radon-emitting alpha particle's energy (5489 keV). For each event, the total signal ($totalSignal$) is calculated by summing up signal of pixels along the same track ($Signal_n$). Fig. 3 shows that 1000 events are large enough for the energy distribution to have a Gaussian-like distribution. A least square fit of Gaussian distribution is performed on the energy spectrum (Fig. 3 red curve), and Full Width at Half Maximum (FWHM) of the Gaussian distribution is used for characterizing energy resolution. Meanwhile, for comparison and quality control, we also calculate the sum of signals without noises ($eventEnergy$), the sum of noises ($noiseSum$), and the sum of noises that have passed the threshold ($noisePassSum$) for each event. The distribution of $eventEnergy$ is a delta-function mounted at 5489 keV, as it should be. In all these graphs, $totalSignal$ shift to a smaller value relative to $eventEnergy$. Since we assume that all energy of an alpha particle has been transfer to energy of electrons, the mean value of the Fig. 3 is meaningless and we will not use it in following discussion.

$$totalSignal = \sum_n Signal_n, \quad (4)$$

$$eventEnergy = \sum_n Hit_Energy_n, \quad (5)$$

$$noiseSum = \sum_n Noise_n, \quad (6)$$

$$noisePassSum = \sum_n (Signal_n - Hit_Energy_n), \quad (7)$$

where $n=1 \dots$ the number of hits of one event.

Fig. 3 shows the distribution of above quantities for four typical pixel size at 2σ threshold, as well as gaussian fitting on distribution of $totalSignal$.

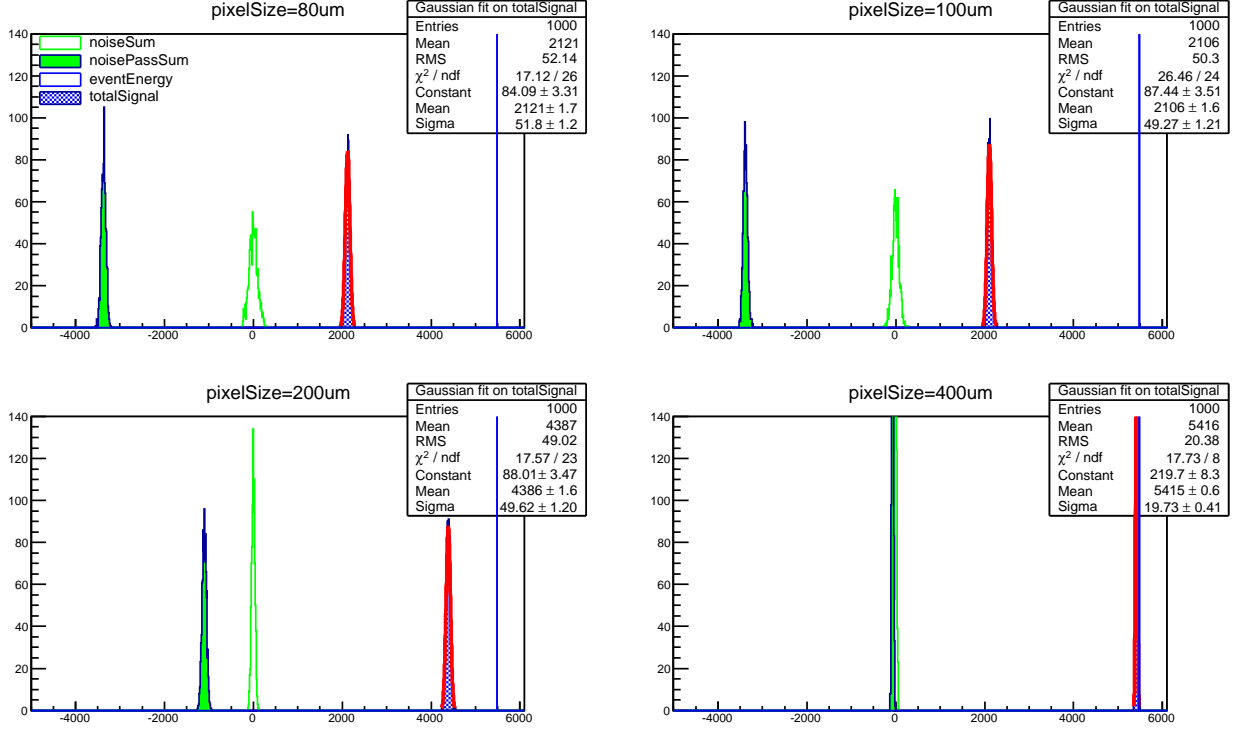


Fig. 3. Total signal (*totalSignal*), total signal without adding noises (*eventEnergy*), sum of noises (*noiseSum*), and sum of noises that have passed the threshold (*noisePassSum*) of 1000 events, with 2σ threshold, for four typical pixel size 80 μm, 100 μm, 200 μm and 400 μm. Gaussian fitting on total signal is indicated by a red curve in each graph. Fitting parameters as well as statistics parameters are listed in the box at top right corner of each graph.

4 Simulation Results

4.1 Energy Resolution vs. Pixel Size

The relationship of energy resolution with pixel size is shown in Fig. 4 (red squares, left axis scale). The threshold is fixed at a typical value 2σ . Given that σ is an intrinsic property of pixel, depending on the standard foundry process and material, we assume that σ is the same for different pixel size that we currently discuss. We observe a general decreasing trend for FWHM for very large pixel size, with a non-monotonic behavior at small pixel size region. This behavior is due to two counter-productive effects. On the one hand, energy resolution becomes better for larger pixels, because larger pixels receive stronger signal leading to improvement of signal to noise ratio. On the other hand, since we record a signal only if the signal is larger than threshold, signals generated by larger pixels have more possibility of passing the threshold, which increases the statistical uncertainty and worsens the energy resolution. However, for very large pixel size, almost all signals are strong enough to pass the threshold, the variation due to the second reason is not so noticeable, thus the graph retrieves a monotonic decreasing trend.

The energy resolution variation due to the second reason can be illustrated by plotting number of hits, i.e. the number of pixels that have signal larger than the threshold, with pixel size (blue dots, right axis scale). Also, to describe this relation, we introduce an empirical expression

$$n = n_0 + \frac{A}{x^2}, \quad (8)$$

where A is the total area that outputs non-zero signals, x is pixel size, and n_0 is a constant due to the fluctuation of noise. A increase as pixel size increases, because larger pixel receives stronger signal, which is favorable for passing the threshold. Thus, A can be expressed by $A = A_0 + A_S$, where A_0 is a constant where the increase starts on. $A_S = A_L / (1 + e^{-k(x-x_0)})$ is a raising logistics function with a limit value A_L , central point x_0 and steepness k . The limit A_L is due to the limited total sensing area for a given event. Fig. 4 shows that this expression fits well with the simulation result of the number of hits with pixel size.

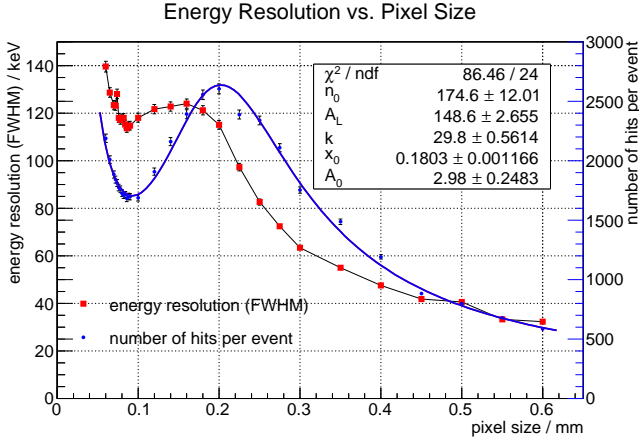


Fig. 4. Energy resolution with pixel size (red squares) and number of hits per event with pixel size (blue dots), with 2σ threshold. The blue line is the fitting line for number of hits per event.

4.2 Energy Resolution vs. Threshold on Pixel

The relationship of energy resolution with threshold on pixel is shown in Fig. 5. Four typical pixel size $80\ \mu\text{m}$, $100\ \mu\text{m}$, $200\ \mu\text{m}$ and $400\ \mu\text{m}$ are examined. From the figure, for pixel size $80\ \mu\text{m}$ and $100\ \mu\text{m}$, energy resolution is significantly better for higher threshold; while for pixel size $200\ \mu\text{m}$ and $400\ \mu\text{m}$, energy resolution is almost the same for all thresholds. There are several intersecting points between lines, meaning that for the same threshold and the same energy resolution, there exists more than one choice of pixel size. Threshold lower than 1σ (the shaded area in Fig. 5) are excluded in our consideration, for ensuring the track finding algorithm's effectiveness. Also, we need to be more careful to exclude data points whose threshold are too high that the detector has potential risk of losing a signal. Maximum valid threshold for a certain pixel size are roughly estimated using maximum signal that are recorded for 2σ threshold. For example, in Fig. 2 we can see the maximum signal for $100\ \mu\text{m}$ and 2σ threshold (labeled "max signal") is about $0.69\ \text{keV}$. Then we divide this number by $0.0337\ \text{keV}$ (energy of one electron) and get ~ 20 electrons that have passed the $2\sigma (= 30\ e^-)$ threshold. From this the maximum number of electrons locate in one pixel is about $50\ e^-$, i.e. 3.3σ . For $80\ \mu\text{m}$ this threshold is found to be 2.8σ . For $200\ \mu\text{m}$ and $400\ \mu\text{m}$ the maximum valid threshold are larger than 4σ . Thus, points that have threshold higher than the corresponding maximum valid threshold (the last four blue squares and the last three red dots in Fig. 5) should be excluded in our consideration.

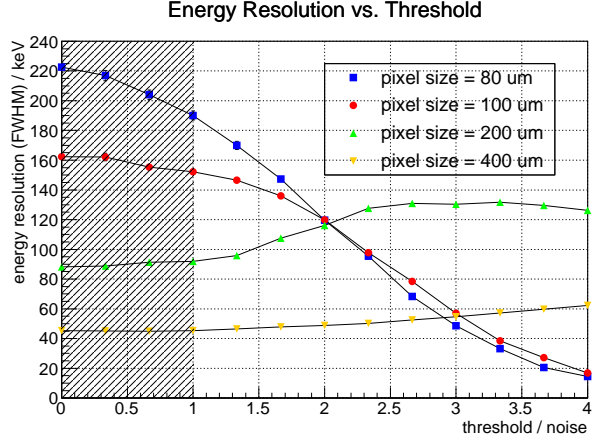


Fig. 5. Energy resolution with threshold on pixel.

Among the valid data points in Fig. 5, we see that the one with pixel size $400\ \mu\text{m}$ at 1σ threshold contributes an energy resolution of $45\ \text{keV}$ FWHM.

5 Conclusion

We study how pixel size influences energy resolution for *Topmetal-II* pixelated radon detector when the pixel size is relatively small, using a simulation method based on Geant4. A non-monotonic behavior of energy resolution with pixel size is observed. It can be shown that this phenomenon is due to the combination effect of pixel size and threshold, by fitting the variation of number of hits with pixel size, using an empirical expression that we introduce.

The contribution of electronic noise to energy resolution for $400\ \mu\text{m}$ pixel size and 1σ threshold is $45\ \text{keV}$ FWHM, which is comparable to the energy resolution causing by energy fluctuation in ionization process ($\sim 20\ \text{keV}$). However, whether we need a larger pixel size for a better energy resolution also depends on the accuracy of differentiating alpha particle under the corresponding pixel size setting. Also notice that this is a simplified model used to study the energy resolution changing by pixel size. More physical processes should be added to learn energy resolution changing with varies parameters.

The authors thank other members in Pixel Lab at Central China Normal University for their valuable discussions.

6 Conflict of Interest

On behalf of all authors, the corresponding author states that there is no conflict of interest.

References

- 1 World Health Organization, *WHO Handbook on Indoor Radon: A Public Health Perspective*, (WHO Press, Geneva, 2009), pp. 3–14
- 2 R. C. Bruno, *J Air Pollut Control Association* **33**(2), pp. 105–109 (1983)
- 3 B. D. McNally, S. Coleman, J. T. Harris, W. K. Warburton. Improving the Limits of Detection of Low Background Alpha Emission Measurements. (ArXiv Preprint, 2017) <https://arxiv.org/abs/1707.09976>
- 4 M. An et al. *Nucl. Instrum. Methods Phys. Res. A*, **810**, pp. 144–150 (2016)
- 5 S. Agostinelli et al. *Nucl. Instrum. Methods Phys. Res. A*, **506**(3), pp. 250–303 (2003)
- 6 S. Biagi, *Magboltz-Transport of Electrons in Gas Mixtures*. (CERN program library, 2000) <http://consult.cern.ch/writeup/magboltz/>